

# Variational mode decomposition linked wavelet method for EMAT denoise with large lift-off effect



Dan Si<sup>a</sup>, Bin Gao<sup>a,\*</sup>, Wei Guo<sup>a</sup>, Yan Yan<sup>a</sup>, G.Y. Tian<sup>a,b</sup>, Ying Yin<sup>c</sup>

<sup>a</sup> School of Automation, University of Electronic Science and Technology of China, China

<sup>b</sup> School of Electrical and Electronic Engineering, Newcastle University, England, UK

<sup>c</sup> Sichuan Special Equipment Inspection Institute, China

## ARTICLE INFO

### Keywords:

Electromagnetic acoustic transducer  
Non-destructive testing  
Ultrasonic echo signal model  
Denoising  
Variational mode decomposition  
Defect detection

## ABSTRACT

Electromagnetic acoustic transducer (EMAT) is an emerging non-destructive testing technique which is widely used in the industry. EMAT has advantages of a non-coupling agent with the capability of big lift-off detection. However, EMAT has an issue of low efficiency in conversion and it is susceptible to noise. This paper proposes a modified variational mode decomposition (VMD) linked wavelet method for EMAT denoising. It enables to suppress both high-frequency narrowband noise and normal noise in EMAT signals with a large lift-off detection condition. In particular, a new ultrasonic echo signal model with a large lift-off influence is proposed for interpretation of denoising mechanism. To investigate the efficacy and the robustness of the proposed method, experimental studies have been carried out for different test samples. A comparative analysis has been undertaken to confirm that the proposed method not only removes the noise but also preserves the information of defect. The Matlab demo code can be linked: [http://faculty.uestc.edu.cn/gaobin/zh\\_CN/lwgc/153392/list/index.htm](http://faculty.uestc.edu.cn/gaobin/zh_CN/lwgc/153392/list/index.htm).

## 1. Introduction

Non-destructive evaluation methods are well applied in the industry [1]. Several well-known Non-Destructive Testing (NDT) methods have been conducted in flaws detection. These include Ultrasonic Testing (UT), X-Ray, Magnetic Particle Testing (MT) techniques, and etc. UT is a mature weld testing NDT technique [2–4]. However, as for piezoelectric transducers, echo amplitude is highly affected by the measurement conditions such as surface roughness [5]. In addition, a coupling agent is required which limits its application. MT can only be used for ferromagnetic materials. In addition, the test specimens should be magnetized [6,7]. X-Ray testing can obtain a good visual result while it has a radiation issue [8,9]. Particularly, MT and X-Ray are difficult to be used for inner pipe detection.

The electromagnetic acoustic transducer (EMAT) is a non-contact NDT method which generates ultrasonic waves in conductive materials [10–13]. Unlike common piezoelectric transducers, a combination of the static and alternating magnetic field is used in EMAT to convert electrical energy into acoustic energy. In particular, EMAT has advantages of non-contact characteristic with good detection rate to overcome issues from the interference due to the rough surface of the specimen. Jin-Hyuk Lee [14] et al. used SH-EMAT to generate SH<sub>0</sub>

guided wave to evaluate the position and size the defects in a welding zone. Wavelet signal processing methods were applied to analyze the received SH-waves signals. Lei Yang et al. [15] used the Laser/EMAT ultrasonic (LEU) technique to measure the weld penetration depths in thick structure based on ray-tracing of the laser-generated bulk as well as the surface waves. However, when the thickness of the measured object, as well as the excitation frequency, are different, the EMAT transducer will generate more than one mode for guide wave. Modes in different frequency-thickness-product have different velocity except for SH<sub>0</sub>. It is difficult to analyze the echo signal which suffers from the interference of the increased mode [14].

In addition, EMAT has issues of low efficiency in conversion and it is susceptible to noise especially when there exists a lift-off distance [16]. Since the signal is corrupted with noise, it will lead to the false alarm in detection. In order to improve the signal-to-noise ratio, the use of noise reduction signal processing methods is a critical step to improve the validity and reliability of the EMAT system. The most common ultrasound signal processing method is a frequency domain analysis. The frequency components can be obtained by using a Fourier transform. However, this process cannot simultaneously collect both time and frequency information. Minhuy Le et al. [17] used the short-time Fourier transform (STFT) to analyze the ultrasonic signal and it

\* Corresponding author.

E-mail address: [bin.gao@uestc.edu.cn](mailto:bin.gao@uestc.edu.cn) (B. Gao).

<https://doi.org/10.1016/j.ndteint.2019.102149>

Received 30 December 2018; Received in revised form 10 July 2019; Accepted 21 July 2019

Available online 26 July 2019

0963-8695/© 2019 Elsevier Ltd. All rights reserved.

successfully detected pitting corrosion cracks in rivets from the multi-layer structure by using an ultrasonic B-scan method. However, STFT has a fixed window size and it cannot yield a good resolution. Kim et al. [18] compared STFT and wavelet transformation (WT). It discovered that WT is a promising method to analyze the acoustic signals. S. Legendre et al. [19] proposed a wavelet-based method to perform the analysis of the received ultrasonic signals during the inspection of the reinforced composite materials. The wavelet transform can simultaneously provide both spectral representation and temporal order of the signal decomposition components to construct a C-scan image. Erdal Oruklu et al. [20] analyzed signal decomposition properties of the discrete wavelet transform (DWT) for enhancing the flaw detection. They presented the performance analysis for different wavelet kernels with respect to ultrasonic NDE applications. Liang Wei et al. [21] proposed a weak ultrasonic signals identification method by using the optimal scale wavelet transform. The selection of the optimal scale is realized by maximizing the negentropy of the DWT coefficients. Besides, wavelet transform and neural network are often combined for defect detection [22]. WU Miao et al. applied wavelet to extract the features of the defected signal. The eigenvalues of the defect are identified by using the amplitude of mean square wavelet in combination with BP neural network to realize the defects classification. F.C. Cruz et al. [23] applied the discrete Fourier Transform (FT), wavelet transform (WT) and cosine transform (CT) to extract features from the tested ultrasonic signal. Statistical techniques such as principal component analysis (PCA) and Wilcoxon-Mann-Whitney (WMH) are used for optimal feature selection. However, wavelet transform requires to choose a proper basis function as well as the decomposition level. Norden E. Huang et al. [24] put forward Empirical Modes Decomposition (EMD) in which it can perform time-frequency signal analysis. Sun M et al. [25] used EMD to deal with an ultrasonic signal to suppress the noise and enhance flaw signals. It was experimentally verified by using a stainless steel pipe with artificial flaws. T Kubik et al. [26] applied EMD to ultrasonic cardiological data and obtained a higher signal to noise ratio. ZHAOHUA WU and NORDEN E. HUANG [27] proposed Ensemble Empirical Mode Decomposition (EEMD) which consists of sifting an ensemble of white noise-added signal and treats the mean as the final result. Zhichao Nie et al. [28] applied the wavelet and EEMD to denoise the ultrasonic signal for highlighting the real frequency domain components. JM Yu et al. [29] proposed EMD and EEMD to analyze the ultrasonic signal because of the non-stationary characteristic of the echo signal. However, when there exists a strong noise in the signal, the problem of ambiguity modes remains detection challenge. In 2014, Dragomiretskiy et al. [30] proposed a non-recursive method variational mode decomposition (VMD) to overcome those problems. The VMD algorithm has been used in various fields. Changfu Liu et al. [31] proposed a novel approach to detect the milling chatter based on VMD and energy entropy. Zhang Xin et al. [32] applied the VMD method to analyze vibration signals from rotating machinery. However, VMD has a problem with the requirement to artificially setting the number of modes in advance. Too large  $K$  will lead to over-segmentation which leads to the break down of the useful signals. On the other hand, too small  $K$  will lead to under-segmentation in which the reduction of noise is not completed. At present, the main approach to determine the appropriate mode number  $K$  is by artificially setting it through the human experience. The echo signal of EMAT is almost the same as the ultrasonic signal. Therefore, the literature review of the signal processing methods of the ultrasonic NDT is also introduced. Several relevant techniques are applied in EMAT as well. These can be referred to as [33,34].

In this paper, a modified VMD linked wavelet denoising method is proposed for electromagnetic ultrasonic NDT. It enables to suppress both high-frequency narrow band noise and white noises in EMAT signals with a large lift-off effect. A kurtosis-based decision rule is presented to determine the effective component. In addition, the linked wavelet de-noising method is employed to reduce the residual white

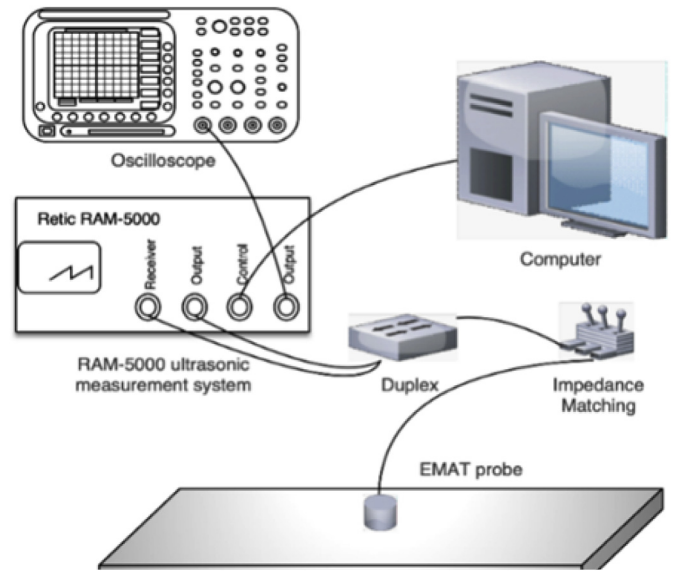


Fig. 1. Diagram of EMAT system.

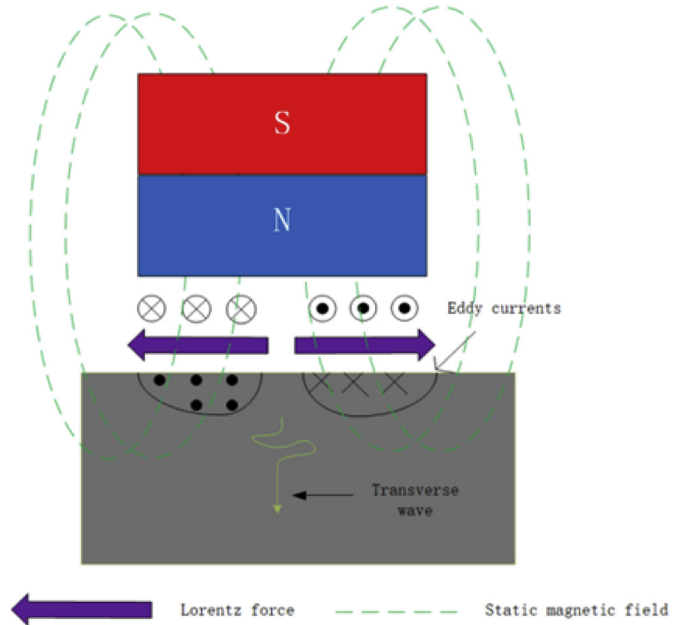


Fig. 2. EMAT transverse wave generation.

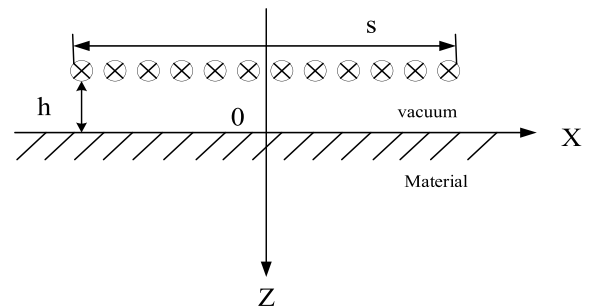


Fig. 3. EMAT transverse wave generation.

noise. The experimental platform and the tested specimens have been conducted to confirm the stability and validity of the proposed method.

The rest of this paper has been organized as follow. Section 2 describes the basic theory of the EMAT and the proposed denoising

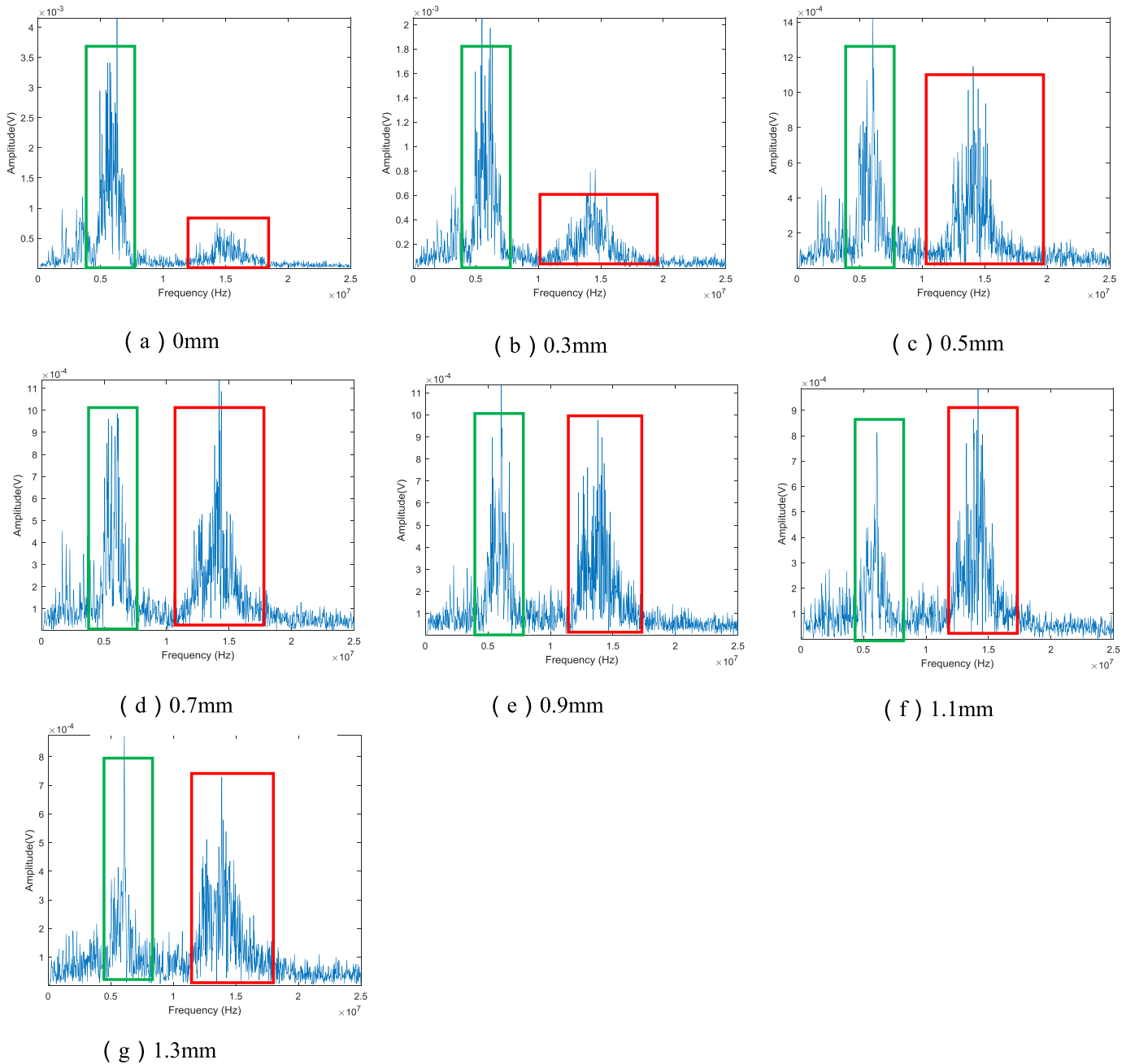


Fig. 4. The frequency spectrum of different lift-off distance.

method. The experiment studies are presented in Section 3. Section 4 concludes the study and outlines future work.

## 2. Methodology

### 2.1. Introduction of the EMAT system

The schematic diagram of the EMAT system is shown in Fig. 1. Electromagnetic ultrasonic testing technology uses electromagnetic effects to stimulate and receive ultrasonic detection. Fig. 2 shows the generation process of the Lorentz Force and the Lorentz is mainly caused by the static field. An alternating current  $I$  is entered in the coil, and the generated magnetic induction intensity  $B_{jb}$  should be satisfied:

$$B_{jb} = \nabla \times A \quad (1)$$

where  $A$  is magnetic potential. An alternating magnetic field is caused

over the test specimen and it will produce eddy currents, namely

$$E = -\frac{\partial A}{\partial t} \quad (2)$$

$$J_w = \gamma E \quad (3)$$

$E$  denotes the electric field that is produced by alternating the magnetic field,  $J_w$  is the eddy currents density.  $\gamma$  is the conductivity of the test specimen. Eddy current will generate Lorentz force  $F$  under the bias magnetic field  $B_0$  provided by permanent magnets and alternating magnetic field. The formula is expressed as follow

$$F = J_w \times (B_0 + B_{jb}) \quad (4)$$

The charged particles inside the test specimen will be subjected to Lorentz force and the surface of the test specimen will undergo high-frequency periodic vibration. Thus, the elastic deformation will occur. Especially, when the external static magnetic field is perpendicular to

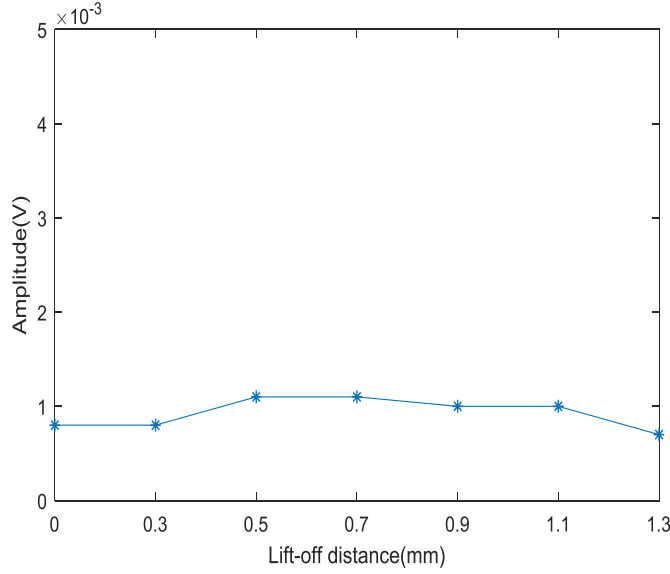


Fig. 5. The amplitude of high-frequency narrowband background in different lift-off distance.

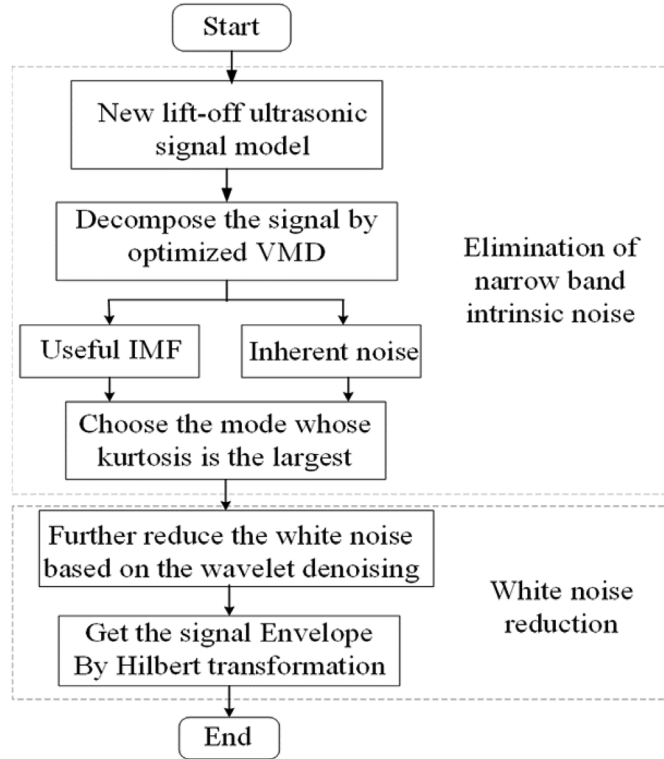


Fig. 6. The flow chart of the proposed denoising method.

the surface of the specimen, the transverse wave will generate. Compared with the static magnetic field, a dynamic magnetic field can be neglected.

When the test specimen is a ferromagnetic material, it is mainly the magnetostriction force and Lorentz forces to produce ultrasonic. More details can be found in Ref. [35].

## 2.2. Proposed methods

Based on the above analysis, ultrasonic echo signal can be used to calculate the thickness or defects detection. However, the safety lift-off

distance between the test sample and probe is required. This distance is necessary for the purpose of the probe protection. In experiments, there always exists the high-frequency narrow band background noise and normal noise in the received echo signal when there is a larger lift-off distance. Therefore, ultrasonic signals are drowned in strong noise.

### 2.2.1. Proposed ultrasonic echo model for lift-off effect analysis

In the EMAT measurement experiment, echo is important because it carries useful information. The echo signal is a time-frequency signal and it is non-stationary. The EMAT signal is almost the same as the ultrasonic signal, and the shape of the both is a tone burst. The traditional mathematical model for the single pulse ultrasonic echo signal can be obtained from the literature, namely

$$x(t) = s(t) + n(t) \quad (5)$$

$$s(t) = \beta e^{-a(t-\tau)^2} \cos(2\pi f_c(t-\tau) + \varphi) \quad (6)$$

In practice, the received echo signal always include noise  $n(t)$  which can be assumed as white Gaussian noise with zero mean and variance  $\sigma^2$  (0,1). Where the phase  $\varphi$  represents the orientation of the reflector and  $\varphi$  is zero in EMAT. The  $\tau$  is related to the thickness of the test specimen.  $\beta$  is the amplitude.  $f_c$  is the center frequency and  $a$  is a bandwidth factor. However, it is different from the traditional signal models when there exists a large lift-off distance. Thus, this paper explores the influence of lift-off distance and a new signal model is proposed.

Fig. 3 shows one basic coil. The coil is not infinite in the  $x$ -derivatives. The length of the coil is  $s$  and has a  $h$  lift-off distance. The electromagnetic and elastodynamic fields are variables in the two-dimensional space of the  $x-z$  plane. The half space  $z > 0$  is filled with a ferromagnetic metal, and the half space  $z < 0$  is filled with a vacuum. It is assumed that the coils with  $n$  turns per unit length along the  $x$  axis and current  $I$  flows the coils. formula (1)-(3) can be written as:

$$\frac{\partial H_x}{\partial z} - \frac{\partial H_z}{\partial x} = J_e \quad (7)$$

$$\frac{\partial E_y}{\partial z} = \mu_0 \bar{\mu}_{xx} \frac{\partial H_x}{\partial t} \quad (8)$$

$$\frac{\partial E_y}{\partial x} = -\mu_0 \bar{\mu}_{zz} \frac{\partial H_z}{\partial t} \quad (9)$$

$$J_y = \eta E_y \quad (10)$$

$$\bar{\mu}_{ij} = 1 + \chi_{ij}/\mu_0 \quad (11)$$

where  $H_x$  denotes the tangential magnetic field,  $H_z$  denotes vertical magnetic field,  $J$  denotes the current density,  $E$  denotes the electric field,  $\mu_0$  denotes the free-space permeability,  $\chi_{ij}$  denotes the magnetic susceptibility tensor, and  $\eta$  denotes the electrical conductivity. formula. (7) can be written as:

$$\left( \frac{\bar{\mu}_{xx}}{\bar{\mu}_{zz}} \frac{\partial^2}{\partial x^2} + \frac{\partial^2}{\partial z^2} \right) H_x - j\omega\eta\mu_0\bar{\mu}_{xx}H_x = 0 \quad (12)$$

Here,  $\omega$  is the frequency which is the same as driving current. For the coil, a current element at  $x$ ,  $nI dx$ , provides the tangential magnetic field at the origin, which can be expressed as:

$$dH_x^V = \frac{nI dx}{2\pi\sqrt{x^2 + h^2}} \cdot \frac{h}{\sqrt{x^2 + h^2}} \quad (13)$$

where  $H_x^V$  denotes the tangential magnetic field in the material and  $h$  denotes the lift-off distance. Thus, the total tangential field at  $z = 0$  caused by the sheet currents is given by:

$$H_x^V = \int_0^s dH_x^V = \frac{nI}{2\pi} \int_0^s \frac{h}{x^2 + h^2} dx = \frac{nI}{2\pi} \arctan \frac{s}{h} \quad (14)$$

where  $s$  denotes the length of the coil and the magnetic field in the material,  $H_x^M$  satisfy formula (13) and the electromagnetic boundary

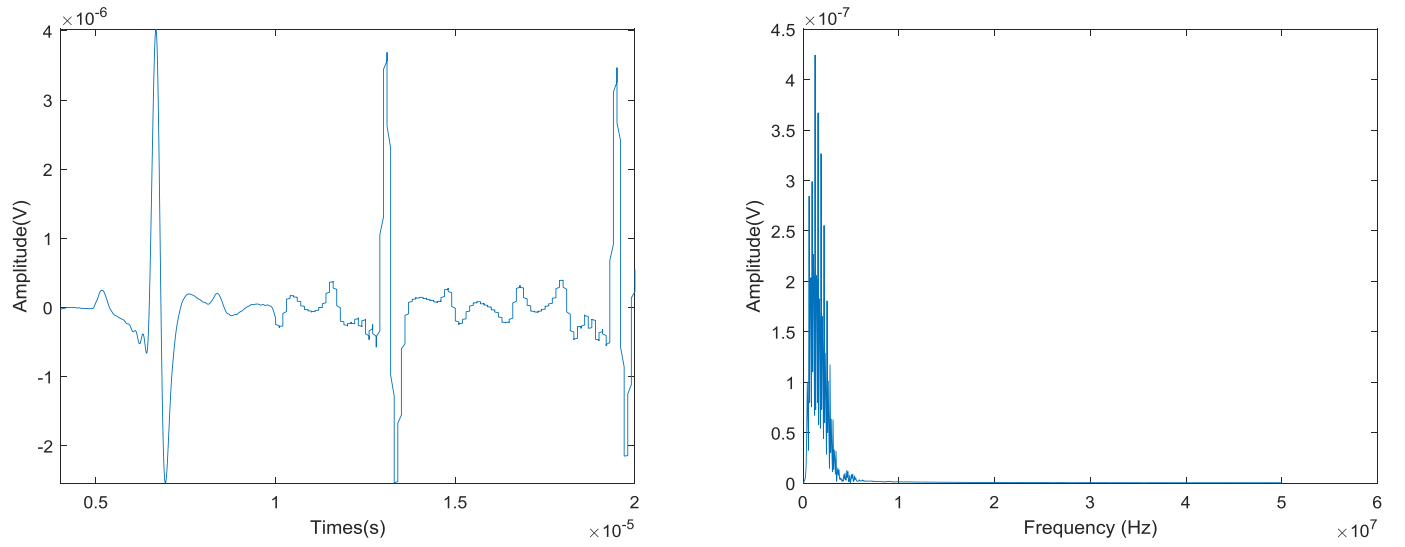


Fig. 7. Original simulation signal.

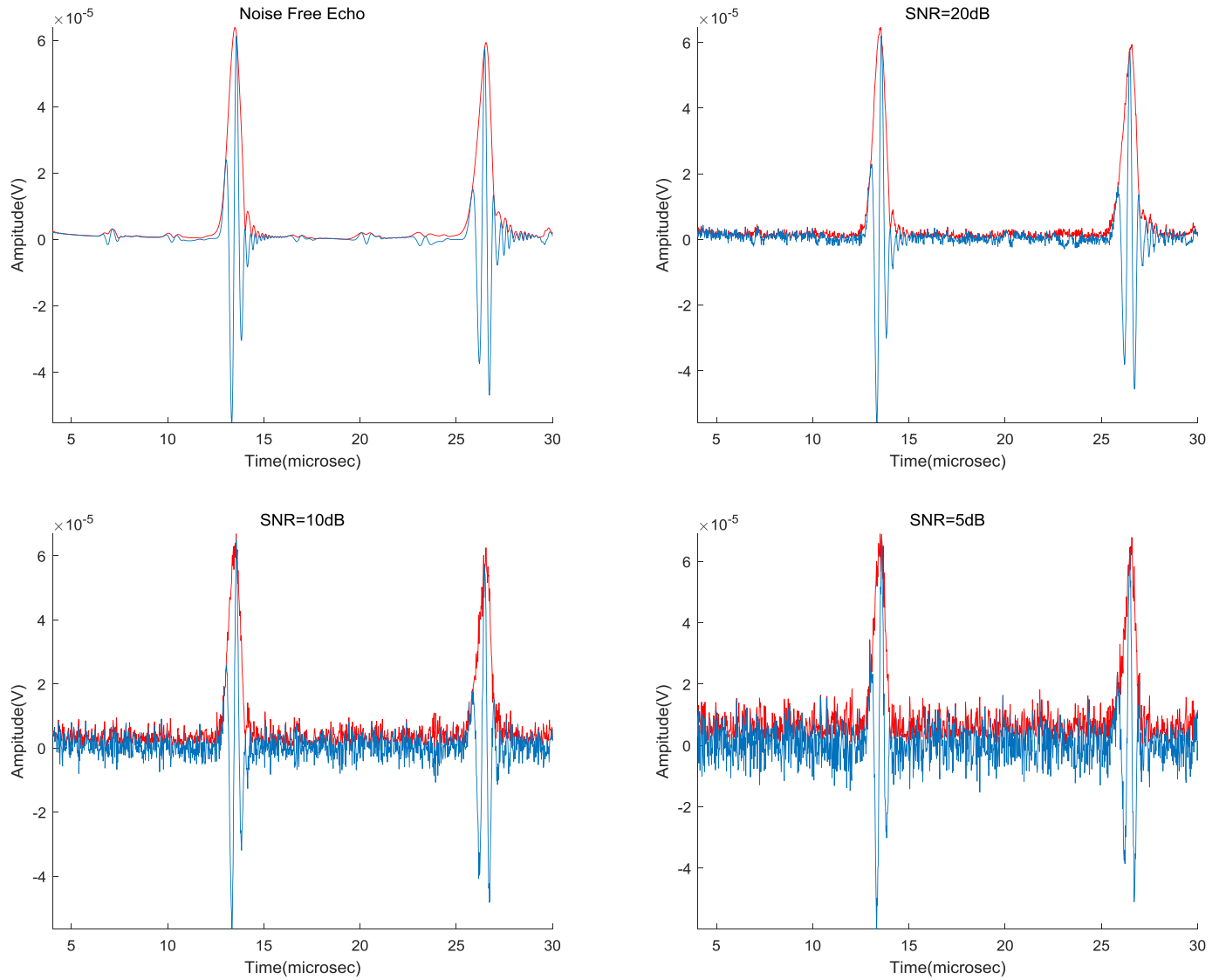
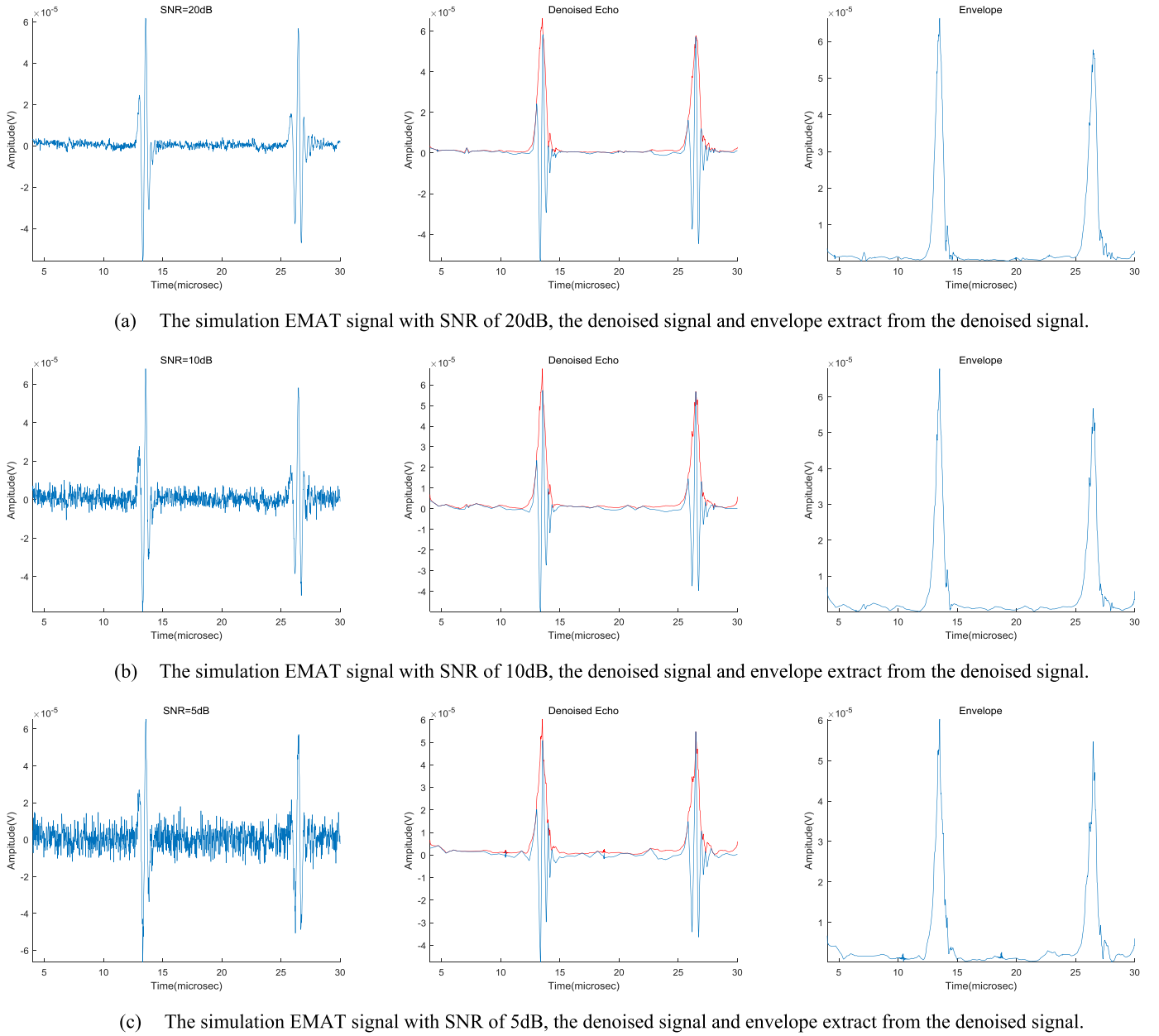


Fig. 8. The simulated EMAT signal with No noise, 5 dB, 10 dB, 20 dB, and the red line is the envelope. (For interpretation of the references to colour in this figure legend, the reader is referred to the Web version of this article.)



**Fig. 9.** Denoising methods based on Hilbert transform and wavelet.

condition at the interface can be given, namely

$$H_x^V(x, 0) = H_x^M(x, 0) = \frac{nI}{2\pi} \arctan \frac{s}{h} \quad (15)$$

Because  $\partial H_x^M / \partial x = 0$  for all quantities, formula (13) can be written as:

$$\frac{\partial^2 H_x^M}{\partial z^2} - q^2 H_x^M = 0 \quad (16)$$

where:

$$q \equiv -\frac{1}{\delta}(1 + j) \quad (17)$$

$$\delta = \sqrt{\frac{2}{\omega \eta \mu_{xx}}} \quad (18)$$

$\delta$  is the electromagnetic skin depth. The solution of formula (16) does not diverge at  $z \rightarrow \infty$  and it satisfies the boundary condition formula (15), namely

$$H_x^M = \frac{nI}{2\pi} \arctan \frac{s}{h} \cdot e^{qz} = \frac{nI}{2\pi} \arctan \frac{s}{h} \cdot e^{-\frac{z}{\delta}} \cdot e^{-j\frac{z}{\delta}} \quad (19)$$

From formula (19), it is easily found that the relationship between the lift-off distance and magnetic field in the material. With the increase of the lift-off, the intensity of magnetic field decay. Form formula (4), the magnitude of Lorentz force is mainly determined by static magnetic field, dynamic magnetic field and eddy current density, respectively. Because the magnitude of the static field is larger than that of the dynamic case, the dynamic magnetic field  $B_{ib}$  can be neglected. Therefore, when the static magnetic field is constant, the amplitude of the Lorentz force mainly depends on the eddy current density. Thus, the lift-off distance plays an important impact on the amplitude of the Lorentz force. Because the variable changes along with the  $z$  axis are much larger than that along with the  $x$  axis, the following relation holds:

$$\left| \frac{\partial H_x^M}{\partial z} \right| \gg \left| \frac{\partial H_x^M}{\partial x} \right| \approx \left| \frac{\partial H_z^M}{\partial z} \right| \gg \left| \frac{\partial H_z^M}{\partial x} \right| \quad (20)$$

formula (7) can be reduced to:



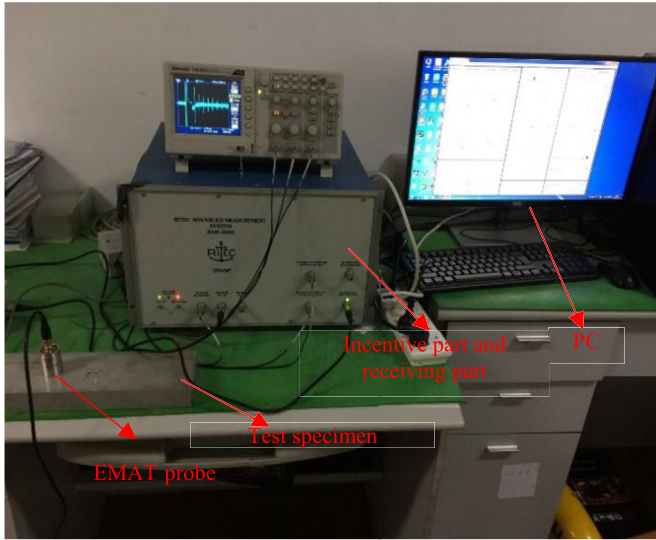


Fig. 10. Experiment set-up.

Table 1  
Test samples.



| Number | Specimen         | Dimension(mm)    | Picture   |
|--------|------------------|------------------|---|
| 1      | 813-X70 pipeline | 425 × 265 × 12.2 |   |
| 2      | Aluminum plate   | 357 × 100 × 35   |  |

Table 2  
Physical parameters of material.

| Parameters                     | value |
|--------------------------------|-------|
| Density (kg/m <sup>3</sup> )   | 7850  |
| Poisson ratio                  | 0.29  |
| Transverse wave velocity (m/s) | 3300  |

Table 3  
Excitation parameters.

| Parameters                | value |
|---------------------------|-------|
| Excitation Frequency(MHz) | 6     |
| Burst Width (cycle)       | 3     |
| Lift height(mm)           | 2.3   |

$$J_e = \frac{\partial H_x^M}{\partial z} \quad (21)$$

Then, the Lorentz forces are:

$$\begin{cases} f_x^{(L)} = B_{0z} \frac{\partial H_x^M}{\partial z} \\ f_z^{(L)} = -B_{0x} \frac{\partial H_x^M}{\partial z} \end{cases} \quad (22)$$

From the above analysis, Lorentz forces are mainly decided by  $\partial H_x^M / \partial z$ . The  $H_x^M$  is decided by not only the driving current  $I$  but also the lift-off distance. With the lift-off distance increasing, the Lorentz force will decay. For ferromagnetic materials, tangential magnetic in the material affects the magnitude of the magnetostrictive force and the

Lorentz force. When lift distance increases, the amplitude of the echo signal decreases which will lead to ultrasound echo to be submerged in noise. However, after extensive experimental verification, the noise of electromagnetic ultrasonic is not only including normal noise but also contains a high-frequency narrowband background noise. In this case study, the frequency spectrums of different lift-off distance are studied as shown in Fig. 4. The excitation frequency is set as 6 Mhz.

In Fig. 4, it can be seen that the high-frequency narrow-band background noise is ranged between 13 Mhz and 16 Mhz and the center frequency is located around 14 Mhz. The high-frequency components exist when there is even no lift-off distance and this can be shown in Fig. 4(a). In this case, the background noise is too small compared with the echo signal, which can be regarded as white noise. Since the lift-off distance increase, the amplitude of echo signal decay and it is close to the amplitude of high-frequency background noise. As shown in Fig. 5, The amplitude of noise basically remains unchanged. However, the energy ratio between the high-frequency narrowband background noise and the excepting echo signal increase with lift-off-distance increase. Thus, the noise is regarded as a certain high-frequency narrowband noise signal and is treated as one Intrinsic Mode Function (IMF). It can be concluded that the characteristics of background noise are approximated as a high-frequency narrow-band signal when there exists a larger lift-off distance.

From the above analysis, this paper proposes a new mathematical model of single pulse ultrasonic echo signal when there exists a large lift-off distance. The model can be expressed as:

$$x(t) = \underbrace{(s(t) + n_1(t))}_{IMF1} + \underbrace{w(t)}_{IMF2} + n_2(t) \quad (23)$$

Here,  $n_1(t)$  denotes the Gaussian white noise in a narrow-band frequency band,  $n_2(t)$  denotes the Gaussian white noise in the whole signal, the  $w(t)$  denotes the high-frequency narrowband background noise and the Intrinsic Mode Functions (IMF) are amplitude-modulated-frequency-modulated (AM-FM) signals.

### 2.2.2. Proposed denoising methods

The schematic diagram of the proposed method is summarized in Fig. 6.

### 2.3. Proposed modified VMD algorithm

The ultrasonic signal is conducted by modified VMD algorithm. VMD algorithm transforms the mode decomposition problem into a variational solution problem and it applies an alternate direction method of multipliers (ADMM) to optimize parameters. In the process of optimization, an ensemble of band-limited Intrinsic Mode Function (IMF) with band-limited is obtained.

Intrinsic Mode Functions are amplitude-modulated-frequency-modulated (AM-FM) signals, namely

$$u_k(t) = A_k(t) \cos(\varphi_k(t)) \quad (24)$$

where the phase  $\varphi_k(t)$  is a non-decreasing function, the envelope is non-negative  $A_k(t) \geq 0$ , on a sufficiently long interval  $[t - \delta, t + \delta]$ ,  $\delta \approx 2\pi / \varphi_k(t)$ , the mode  $u_k(t)$  can be considered to be a pure harmonic signal with amplitude  $A_k(t)$  and instantaneous frequency  $\varphi_k(t)'$ .  $u_k(t)$  is an input of Hilbert transformation to get the signal envelope.

The EMAT signal is a time-frequency signal. The simulated EMAT signal is shown in Fig. 7. The excitation frequency is set as 2 Mhz and aluminum is chosen as the test example. In Fig. 7, it is easily found that the frequency spectrum is the same as the incentive frequency and it is a band-limited signal. Besides, the high-frequency narrowband background noise is a band-limited signal as well. Therefore, EMAT signal and high-frequency narrowband background noise can be considered as a model of Intrinsic Mode Function and it can be separated by a modified VMD algorithm.

The structure of the VMD algorithm is shown as follow:

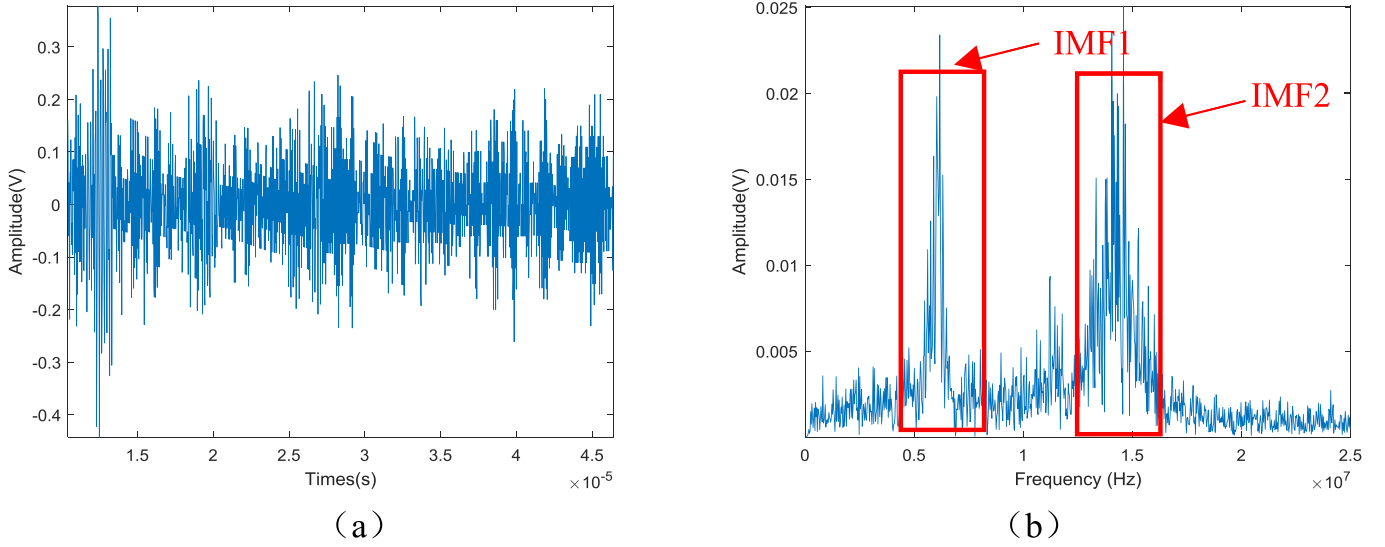


Fig. 11. Original ultrasonic signal. (a) Time-domain waveform and, (b) Single side spectrum.

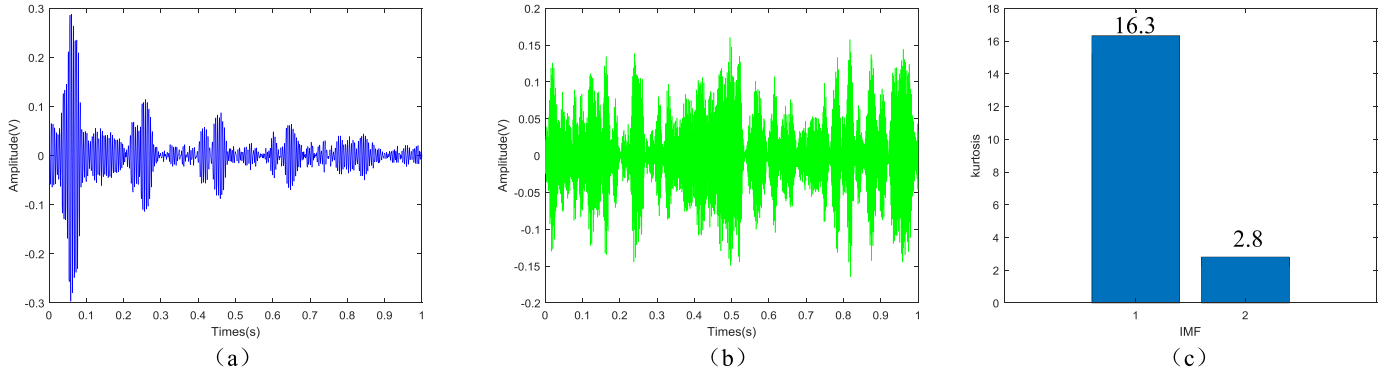


Fig. 12. The modes. (a) the first mode IMF1, (b) the frequency spectrum of IMF1, (c) the second mode IMF2, (d) the frequency spectrum of IMF2, (e) the kurtosis of IMF1 and IMF2.

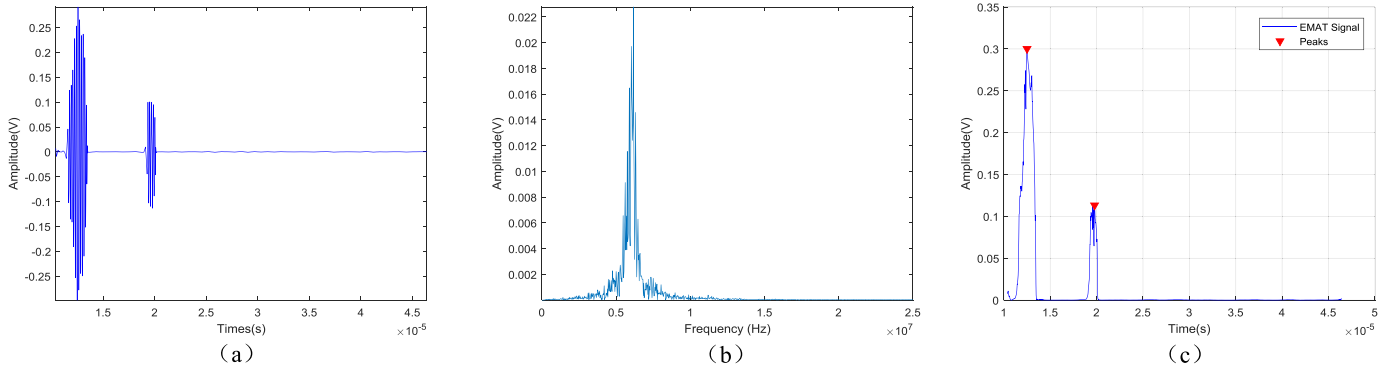


Fig. 13. (a) the signal processed by proposed denoised method, (b) the frequency spectrum of the denoised signal, (c) the envelope of denoised signal.

$$\min_{\{u_k\}, \{w_k\}} \left\{ \sum_k \|\partial_t \left[ \left( \delta(t) + \frac{j}{\pi t} \right) \times u_k(t) \right] e^{-jw_k t}\|_2^2 \right\}$$

$$s. t. \sum_k u_k = f \quad (25)$$

where  $K$  is the number of modes,  $w_k$  is the center frequency of  $u_k(t)$ . The constraint is that the sum of modes is equal to the original signal [30]. suggests that it can introduce a quadratic penalty term  $a$  and Lagrangian multipliers  $\lambda$  in order to make the model unconstrained. The weight of the penalty term is  $a$  inversely proportional to the noise level in the data. Namely, in a strong noise environment, the weight needs to be small in order to enforce strict data fidelity. Lagrangian multipliers is

a common way of enforcing constraints strictly. Thus, the augmented Lagrangian formula is expressed as:

$$L(\{u_k\}, \{w_k\}, \lambda) = a \sum_k \|\partial_t \left[ \left( \delta(t) + \frac{j}{\pi t} \right) * u_k(t) \right] e^{-jw_k t}\|_2^2$$

$$+ \|f(t) - \sum_k u_k(t)\|_2^2 + \langle \lambda(t), f(t) - \sum_k u_k(t) \rangle \quad (26)$$

Through a series of mathematical transformations, the problem is presented as the following:



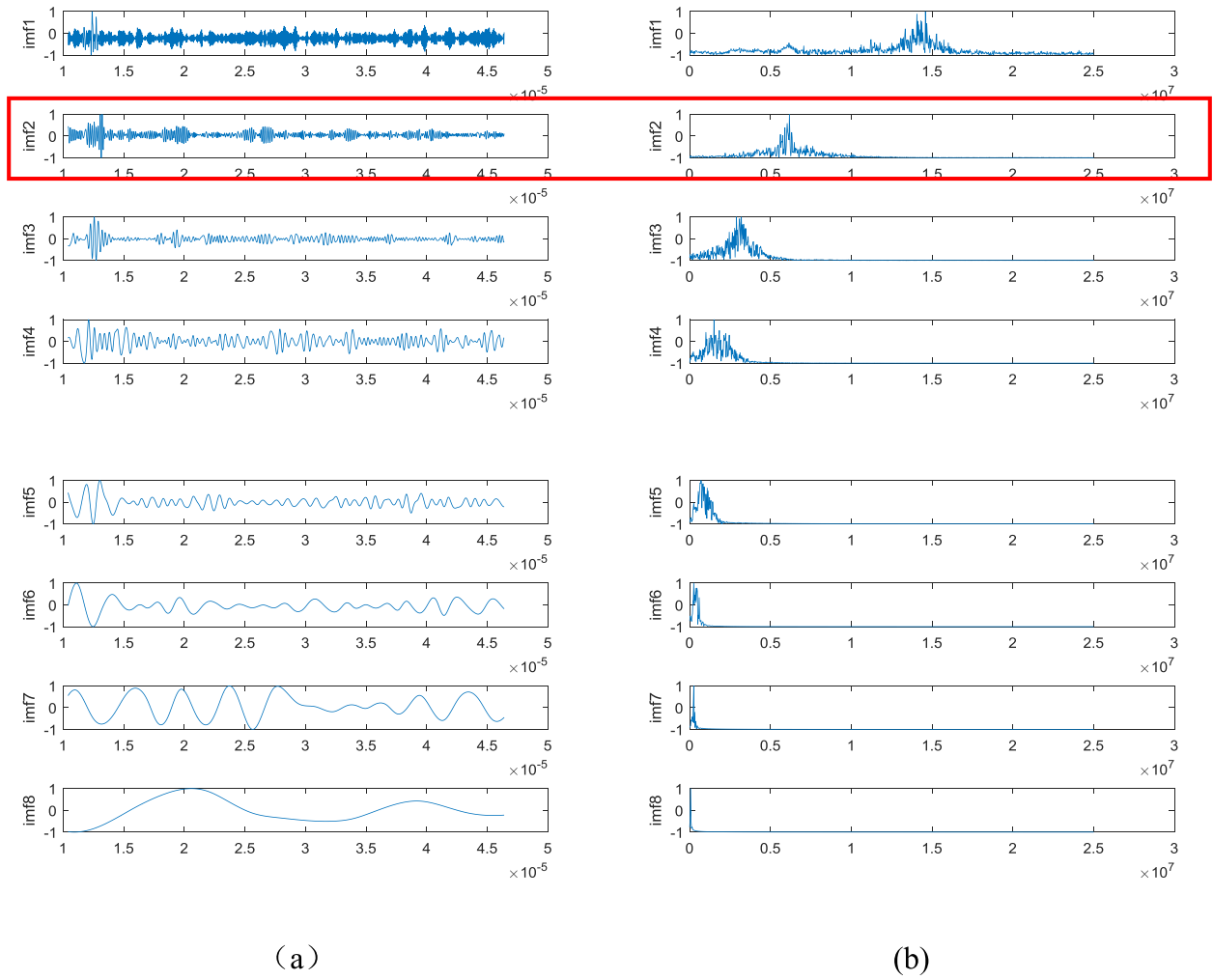


Fig. 14. The phenomenon of modal aliasing processed by EMD algorithm (a) Time-domain (b) Frequency domain.

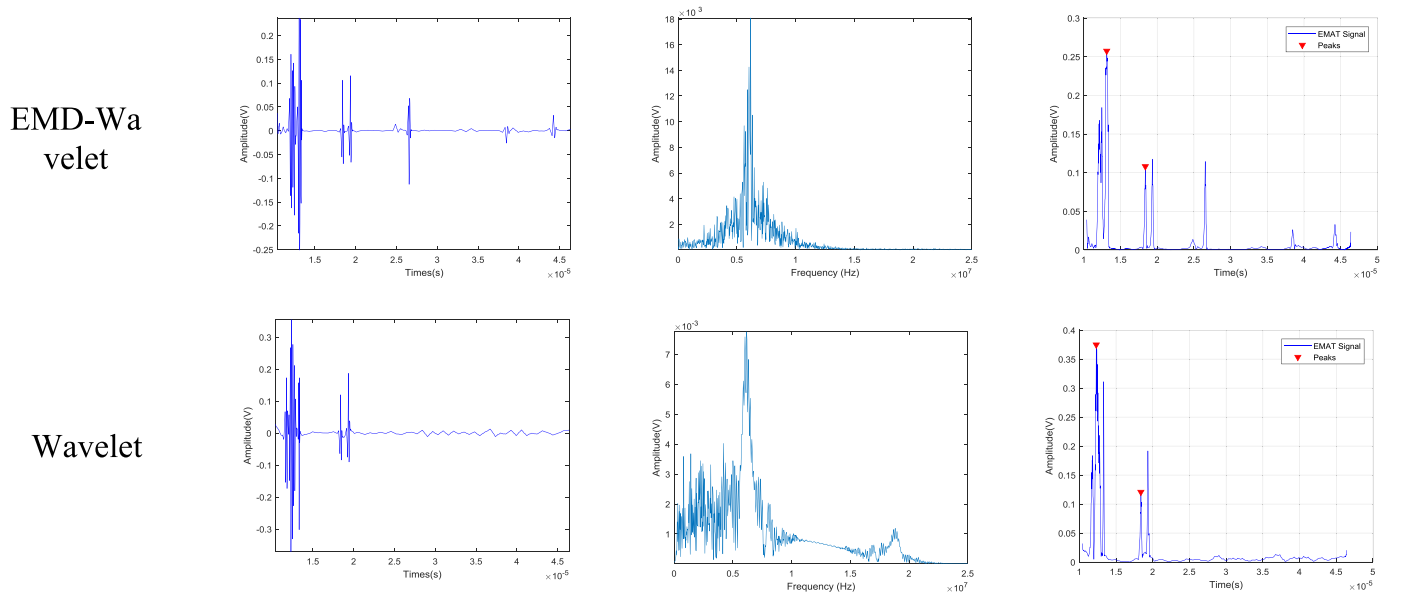


Fig. 15. The signal processed by EMD-Wavelet denoising algorithm and Wavelet denoising algorithm.

**Table 4**  
Performance comparison of the proposed method and the wavelet shrinkage method.

| Denosing Method | SNR       | MSE    | Thickness | Error |
|-----------------|-----------|--------|-----------|-------|
| Wavelet         | -8.82 db  | 0.0072 | 10.0 mm   | 18.0% |
| EMD- Wavelet    | -11.46 db | 0.0074 | 8.7 mm    | 28.6% |
| proposed method | -7.18 db  | 0.0067 | 11.8 mm   | 3.2%  |

**Table 5**  
Physical parameters of material.

| Parameters                     | value |
|--------------------------------|-------|
| Density (kg/m <sup>3</sup> )   | 2.70  |
| Poisson ratio                  | 0.32  |
| Transverse wave velocity (m/s) | 3184  |

**Table 6**  
Excitation parameters.

| Parameters                | value |
|---------------------------|-------|
| Excitation Frequency(MHz) | 2     |
| Burst Width(cycle)        | 3     |
| Lift height(mm)           | 1.5   |

$$u_k^{n+1}(w) = \frac{f(w) - \sum_{i \neq k} u_i(w) + \frac{\lambda(w)}{2}}{1 + 2\alpha(w - w_k)^2} \quad (27)$$

$$w_k^{n+1} = \frac{\int_0^\infty w |u_k(w)|^2 dw}{\int_0^\infty |u_k(w)|^2 dw} \quad (28)$$

More detail of the derivation can be found in Ref. [30]. The choice of parameters is important. In this paper, the quadratic penalty term  $\alpha$  is set to a moderate value 2000, which is recommended by Ref. [30] to get better convergence and the Lagrangian multiplier is set to a moderate value 0 due to the strong noise. Traditional VMD algorithm is required to set the value of the  $K$  in advance. This means that the signal will be decomposed into  $K$  modes. The selection of the  $K$  parameter in the traditional method is decided by human experience or adaptive algorithm. However, there is no reasonable explanation. In this paper, the model in (23) contains two IMFs and it could apply the VMD algorithm

with fixed parameters  $K = 2$  to decompose lift-off EMAT signal. Because the VMD algorithm has the advantage of noise suppression, the signal can be decomposed into two IMFs. One is ultrasound echo signal with white noise, and the other is high-frequency narrowband background noise.

#### 2.4. Select the effective modes

Firstly, the EMAT signal is decomposed into two narrow-band IMFs based on the modified VMD algorithm. Due to the characteristics of ultrasonic signals, the mode which contains ultrasonic signal information should be selected. In the ultrasonic echo signal, every echo signal is a kind of pulse-type signals. Therefore, the effective component of the EMAT signal is defined as a narrow-band signal that owns the characteristics of the sharp rising edge. The kurtosis can effectively indicate the abrupt change of a signal. Kurtosis value of a signal  $x_k$  ( $k = 1, \dots, N$ ) can be computed by the following formula:

$$\gamma_4 = \frac{E(x_k - \mu)^4}{\sigma^4} \quad (29)$$

where the  $E$  is the expectation operator  $\mu$  and  $\sigma$  is the mean and standard deviation of the signal.

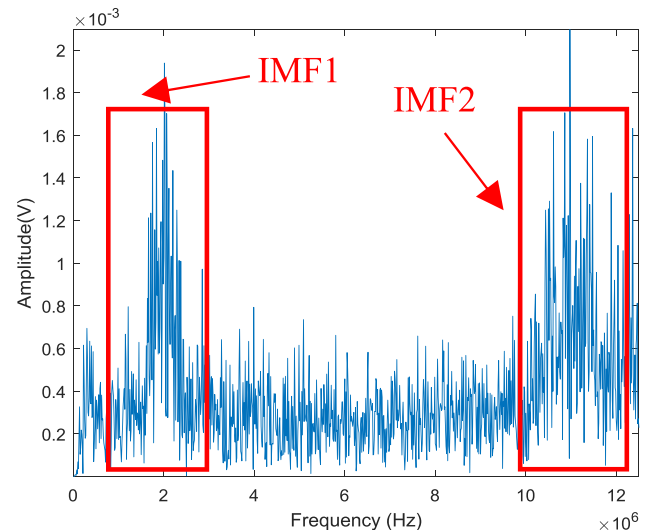
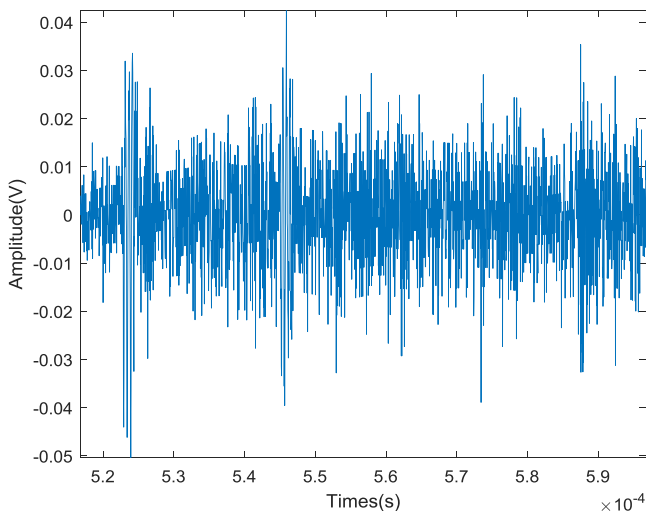
In the IMFs, one IMF is the high-frequency narrowband background noise, and the other contains an effective ultrasonic signal. Therefore, the IMF whose kurtosis is the largest will be selected.

#### 2.5. Elimination of white noise

In this paper, the process of elimination for white noise contains a two-stage process:

- (1) Wavelet denoising is adopted to reduce the noise of the selected IMF.
- (2) The envelope of the ultrasonic signal will be extracted by the Hilbert transform.

In the narrow-band IMF, there still exists white noise. Wavelet transform preserves the local useful information of the signal and removes the noise. The 'db3' wavelet is chosen and the decomposition level is set to 5. These selections are based on experiments which repeated in many realizations. In addition, the noise level estimation of each level of the wavelet decomposition is adjusted and with the rule 'sqtwolog'. The threshold adaptively is expressed as:



**Fig. 16.** Original ultrasonic signal. (a) Time-domain waveform and, (b) Single side spectrum.

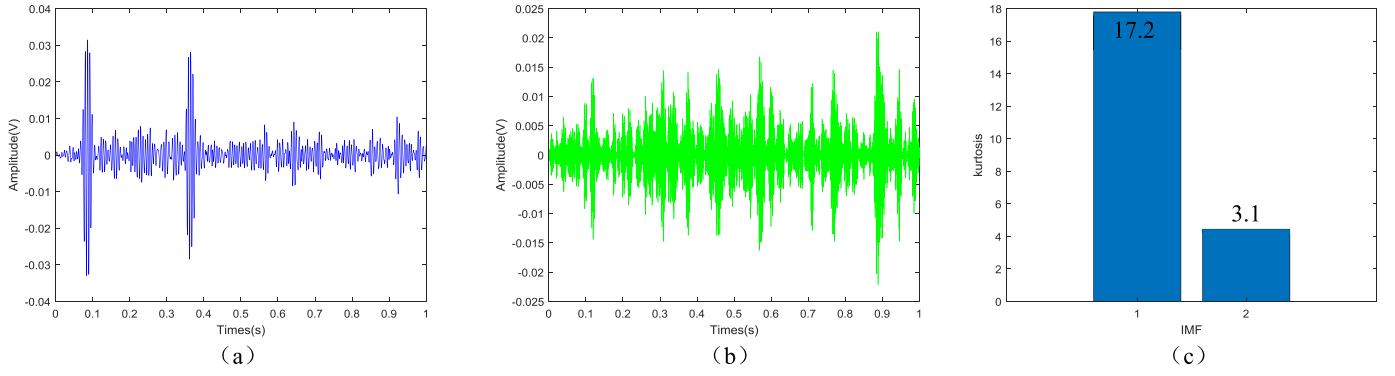
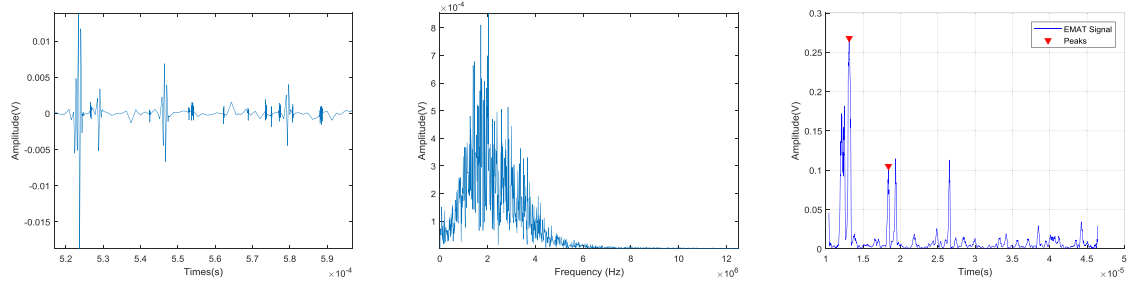
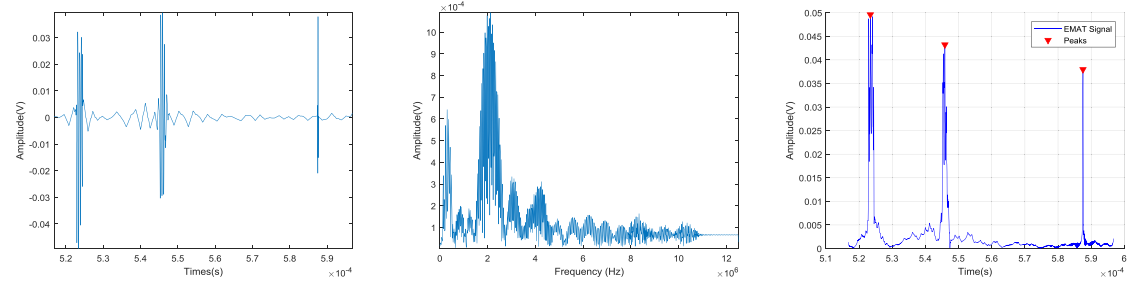


Fig. 17. The modes. (a) the first mode IMF1, (b) the frequency spectrum of IMF1, (c) the second mode IMF2, (d) the frequency spectrum of IMF2, (e) the kurtosis of IMF1 and IMF2.

EMD-Wa  
velet



Wavelet



Proposed  
method

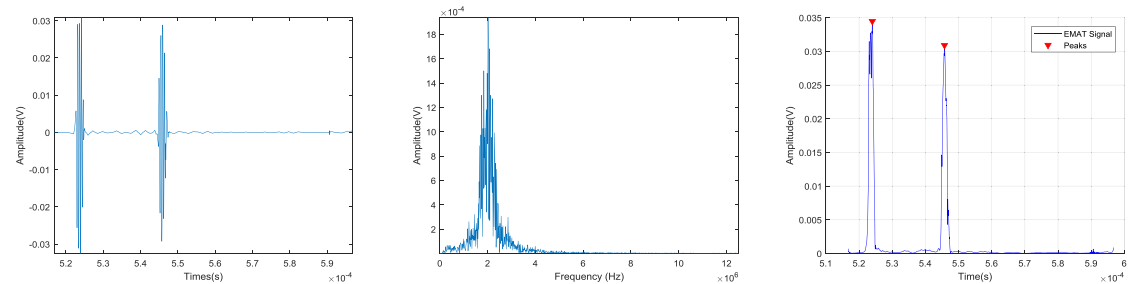


Fig. 18. The signal processed by EMD-Wavelet denoising algorithm, Wavelet denoise algorithm, and the proposed method.

Table 7

Performance comparison of the proposed method and the wavelet shrinkage method.






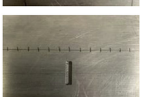
| Denosing Method | SNR       | MSE      | Thickness | Error |
|-----------------|-----------|----------|-----------|-------|
| Wavelet         | −6.34 db  | 0.000095 | 36.0 mm   | 2.8%  |
| EMD- Wavelet    | −18.37 db | 0.00012  | 36.7 mm   | 4.8%  |
| proposed method | −8.16 db  | 0.000097 | 34.6 mm   | 1.1%  |

$$thr_j = \sqrt{2 \log(N_j)} \quad j = 1, \dots, J \quad (30)$$

where  $thr_j$  denotes the threshold of the  $j$ th level, and the  $N_j$  is the number of wavelet coefficients of the  $j$ th level. the hard-thresholding can preserve the characteristics of the signal and it can be used to reduce the white noise. Besides, discrete WT is used.

Hilbert transform can present the instantaneous amplitude and frequency of the signal. The input signal of the Hilbert transform is required to be linear steady state. However, in a real situation, most of the signals are linear unsteady or even non-linear unsteady. Linear steady-state conditions strictly restrict the use of Hilbert transform. The EMD algorithm proposed by HUANG [24] is used to transfer the time-

**Table 8**  
Samples.

| Number | Specimen  | Defect Dimension (mm) | The thickness of defect to the surface (mm) | Picture   |
|--------|---|-----------------------|---|---|
| 1      |  | 40 × 7 × 4.2          | 5.8   |  |
| 2      |  | 20 × 5 × 2            | 16  |  |
| 3      |  | 20 × 2 × 2            | 18  |  |

**Table 9**  
Measurement of different sample defect thickness under different lift-distance.

| Sample | Lift-distance (mm) | Actual thickness (mm) | Calculated thickness (mm) | Error rate |
|--------|--------------------|-----------------------|---------------------------|------------|
| 1      | 0.5                | 5.8                   | 5.7                       | 1.7%       |
| 1      | 0.7                | 5.8                   | 5.6                       | 3.4%       |
| 1      | 0.9                | 5.8                   | 6.1                       | 6%         |
| 1      | 1.1                | 5.8                   | 6.2                       | 6.8%       |
| 1      | 1.3                | 5.8                   | 5.6                       | 3.4%       |
| 2      | 0.5                | 16                    | 15.9                      | 0.6%       |
| 2      | 0.7                | 16                    | 16                        | 0%         |
| 2      | 0.9                | 16                    | 15.9                      | 0.6%       |
| 2      | 1.1                | 16                    | 16                        | 0%         |
| 2      | 1.3                | 16                    | 15.9                      | 0.6%       |
| 3      | 0.5                | 18                    | 18.3                      | 1.6%       |
| 3      | 0.7                | 18                    | 18.2                      | 1.1%       |
| 3      | 0.9                | 18                    | 18                        | 0%         |
| 3      | 1.1                | 18                    | 17.8                      | 1.1%       |
| 3      | 1.3                | 18                    | 18.3                      | 1.6%       |

domain signal into a linear steady state. VMD algorithm can obtain linear steady-state signals which the decomposed IMF has a better performance. Therefore, the decomposed signal is used as an input of the Hilbert transform to obtain the envelope.

The performance of the denoising methods based on wavelet and Hilbert transform are shown in Fig. 8 and Fig. 9, respectively. The simulated EMAT signal is embedded in White Gaussian Noise with a signal-to-noise ratio (SNR) of 5 dB, 10 dB, 20 dB, respectively.

Fig. 8 illustrates the process of ultrasonic echo signal with the Hilbert transform. In Fig. 8, it is obvious that the presence of noise will have a worse impact on the envelope extraction. The envelope that is extracted from the noise-free echo match the original signal. When SNR is low, the envelope cannot match the original signal well and it is not smooth. In conclusion, the accuracy rate of the recovered envelope will decrease with the lower SNR.

To achieve a better envelope, a wavelet denoising method is adopted to eliminate white noise. The denoised results with different level are shown in Fig. 9. The extracted envelope from the denoised signal is smoother and has higher accuracy than the envelope extracted from a signal with noise. At the same time, the envelope extracted from the denoised signal is almost the same as the original envelope without noise. Furthermore, the peak of the extracted envelope with different SNR is always the same, and the local features of the ultrasonic signal are preserved.

## 2.6. Thickness calculation

In this paper, the accuracy of the thickness measurement is denoted as a new indicator to validate the performance of the algorithm. Since the peak time can be extracted from the envelope to calculate the thickness and the energy of the electromagnetic wave are gradually attenuated, the time difference between the first and the second echo signal peak is extracted. The formula can be expressed as:

$$h = v \times t/2 \quad (31)$$

where  $h$  denotes the thickness,  $v$  represents the speed of the transverse wave in the test specimen.  $t$  represents the first and second peak time difference.

## 3. Experiment and result analysis

### 3.1. Experiment set-up

For data acquisition, an experimental platform of EMAT is shown in Fig. 10. It consists of three parts, the incentive part, the receiving part, and the computer control section. The system uses Ritec RAM-5000-SNAP as the electromagnetic ultrasonic excitation source. High-power audio pulse can be set up to 5 KW and the maximum frequency can reach 7 Mhz. It takes reflection mode.

In this paper, the proposed algorithm is used to measure the different materials and defect detection. The intensity of echo generated by electromagnetic ultrasound is different from that of the different materials.

### 3.2. Detection of different materials

#### 3.2.1. Test specimen

In the experiment set up, both ferromagnetic and nonferromagnetic materials have been used in larger lift-off distance. These include 813-X70 pipeline and aluminum plate. The detailed information of these samples can be found in Table 1.

#### 3.2.2. Result and analysis

In 813-X70 pipeline, the material is iron, properties of materials are shown in Table 2 and the setting of excitation parameters is shown in Table 3. Before the experiment, sweep frequency is validated for the tested object to get the maximum amplitude of the echo signal when there is no lift-off distance. As for different tested object whose, physical properties and thickness are different, excitation frequency is selected different to get the maximum amplitude when there is no lift-off distance. In this study, 6 Mhz is chosen as the optimal excitation frequency to get the maximum amplitude for the 813-X70 pipeline. One example of time-domain waveform with 2.3 mm lift-off distance and the spectrum diagram of the original signal is shown in Fig. 11. As shown in Fig. 11, it is difficult to find an ultrasonic echo in the time-domain waveform. The ultrasonic signal is submerged in the high-frequency narrowband background noise signal and white noise.

In Fig. 11(b), the EMAT echo signal with larger lift-off distance satisfies the new proposed model and can be decomposed into two IMFs by using the modified VMD algorithm. Kurtosis is an indicator of the choice of an effective mode, which is calculated and shown in Fig. 12(c). The first mode IMF1 with the maximum kurtosis index (kurtosis = 16.3) is selected as an effective mode. Therefore, the mode IMF1 is selected as an ultrasonic echo signal. The second mode IMF2 is high-frequency narrowband background noise. It is obvious that the IMF remains strong white noise from Fig. 12(a). Therefore, the proposed denoising method is adopted to eliminate the noise. The result is presented in Fig. 13.

It is obvious that the proposed method has the capability to eliminate the noise. At the same time, the frequency of the denoised signal is the same as the excitation frequency. The envelope of the denoised

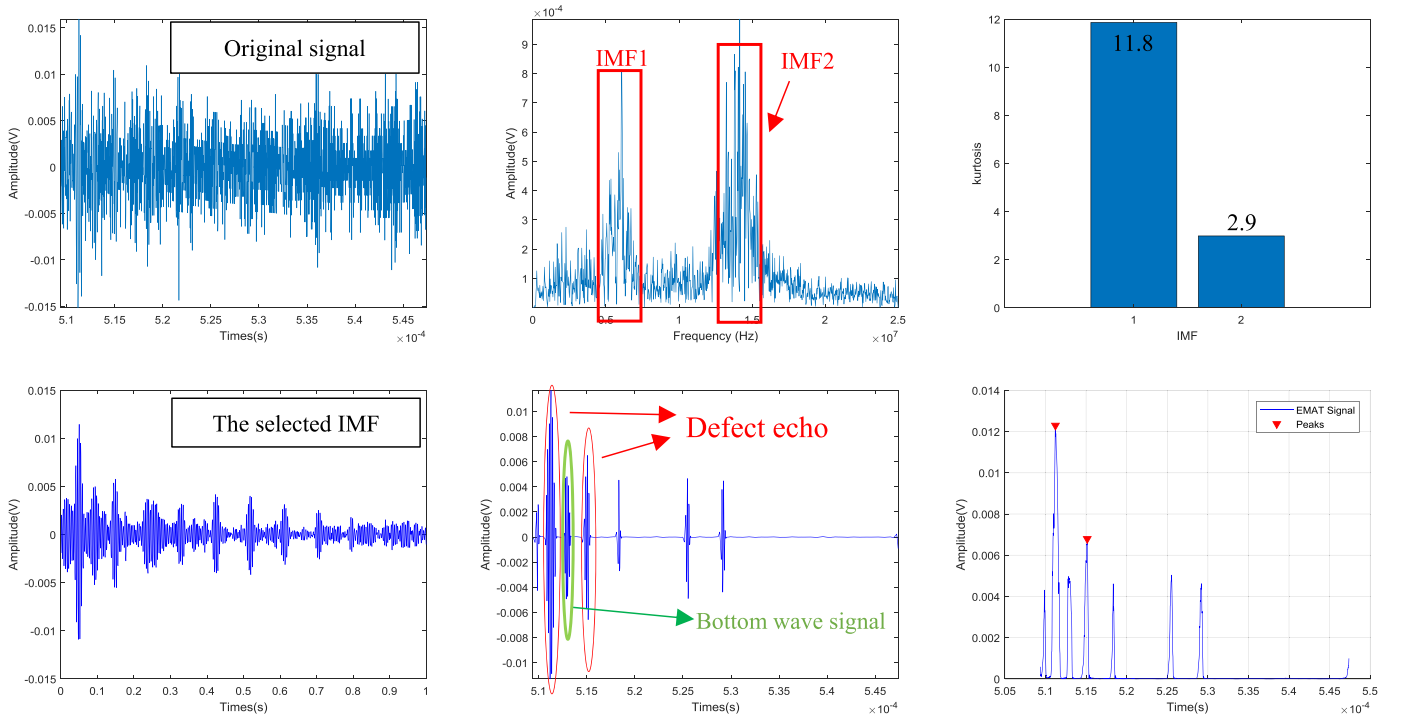


Fig. 19. The echo signal of Sample1 is processed by proposed methods.

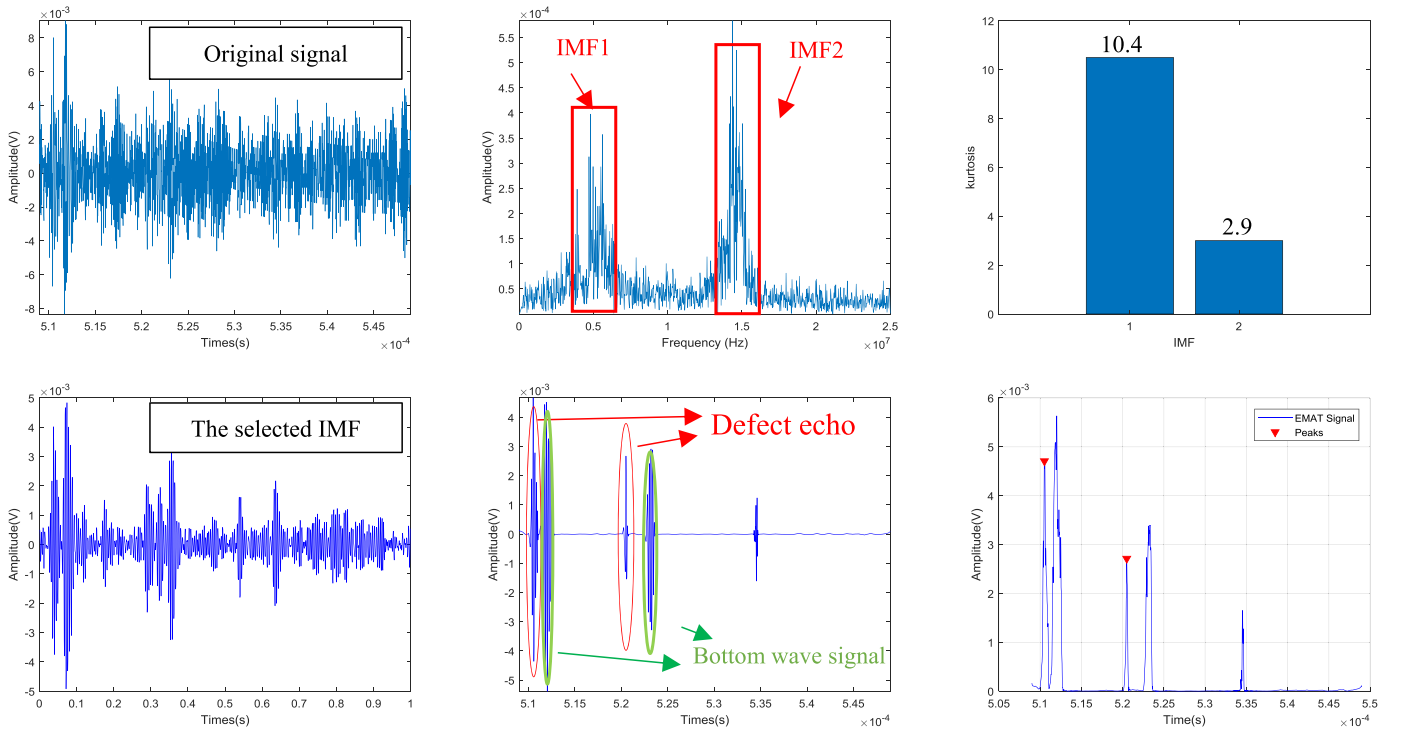


Fig. 20. The echo signal of Sample2 is processed by proposed methods.

signal is represented in Fig. 13(c), and local features of ultrasonic are preserved. In comparison, the EMD-wavelet denoising algorithm and Wavelet denoising algorithm are employed to conduct the denoise process with 2.3 mm lift-off. The common evaluation indexes SNR, mean square error (MSE) and thickness of measurement are employed. As for the EMD algorithm, the phenomenon of mode aliasing exists in several decomposed IMFs. For example, the IMFs that are shown in Fig. 14 indicates the phenomenon of the modal aliasing. Fig.15 shows the denosing comparison performance.

In Fig. 14, it can be seen that EMD cannot efficiently remove the DC interference. In this study, the IMF2 whose center frequency is the same as the excitation frequency is selected. The result is shown in Table 4. The SNR of the proposed method is increased by 18% and 37%, respectively compared with the first two methods. In addition, the envelope obtained by the first two methods has many noises. Meanwhile, there will be several peaks that will disturb the judgment. The true thickness of the pipeline is 12.2 mm. This experiment calculates the time difference between the first wave and the second peak. From the

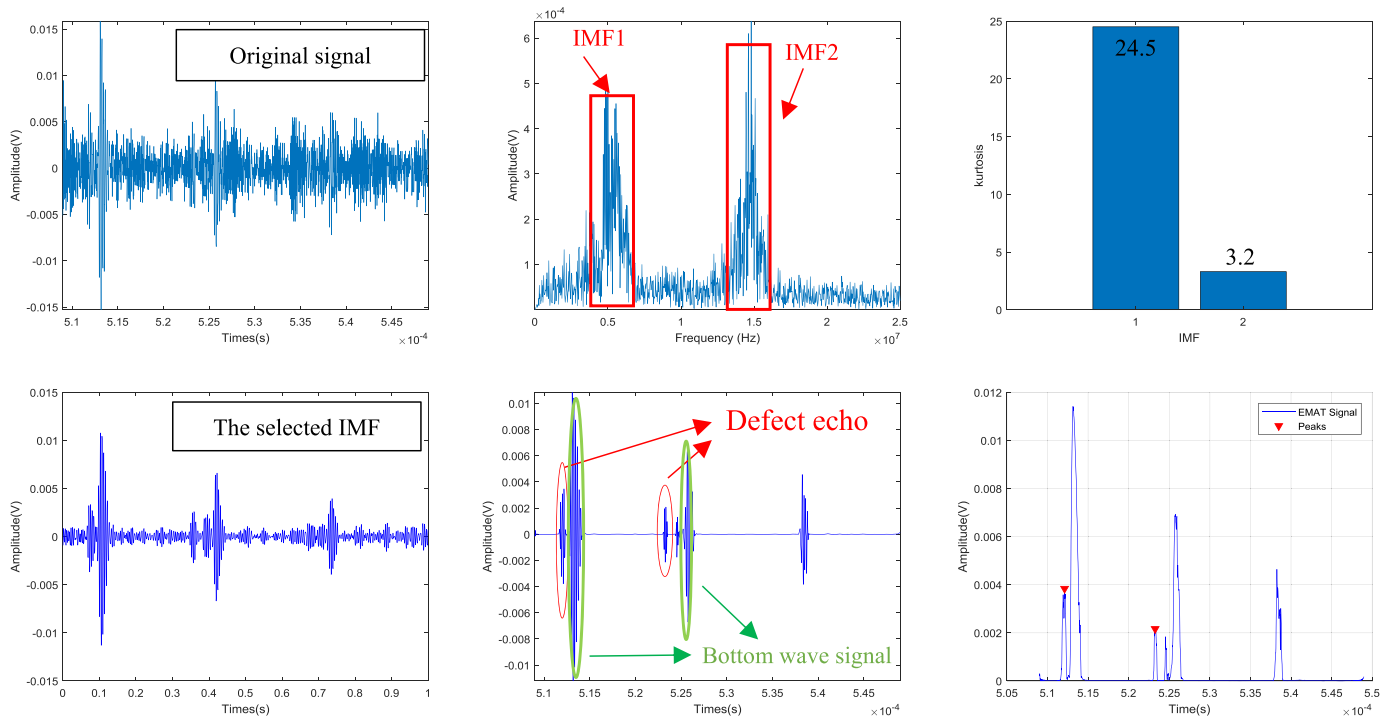


Fig. 21. The echo signal of Sample2 is processed by proposed methods.

comparison result in Table 3, it is obvious that the proposed method has superiority in terms of noise reduction especially in thickness feature extraction.

The excitation mode of electromagnetic ultrasonic on aluminum plate is mainly Lorenz force. Properties of materials are shown in Table 5 and the setting of excitation parameters are shown in Table 6. Before the experiment, sweep frequency is validated for the tested object to get the maximum amplitude of the echo signal when there is no lift-off distance. In this study, 2 Mhz is chosen as the optimal excitation frequency for this aluminum plate. In certain experiments, the optimal frequency for aluminum and steel is the same. In this study, 2 Mhz for the aluminum test can get better SNR than that of using 6 Mhz whereas 6 Mhz can still work. In addition, it is used to validate that the proposed algorithm is applicable to any condition rather than a fixed excitation frequency. Different excitation frequencies will lead to different center frequencies of ultrasonic echo signals. In addition, the energy of ultrasound will decrease with the decrease of the excitation frequency. Therefore, the maximum lift-off distance is 1.5 mm in the aluminum material.

The time-domain waveform with 1.5 mm lift distance and spectrum diagram of the original signal is shown in Fig. 16.

The proposed method is applied to analyze the signal. The IMFs that are decomposed by the proposed method and the kurtosis of each IMFs are shown in Fig. 17.

It is obvious that there is no model aliasing phenomenon. The first model IMF1 with the maximum kurtosis index (kurtosis = 17.2) is selected as an effective mode. In addition, the center frequency of the IMF model is the same as the excitation frequency. The second model IMF2 is high-frequency narrowband background noise. In comparison, the EMD-wavelet method, wavelet denoising have been involved to process the ultrasonic signal with 1.5 mm lift-distance. Hilbert transform is used to calculate the time difference between two echo peaks. The result is shown in Fig. 18.

The true thickness of the aluminum plate is 35 mm. From the comparison result in Table 7, it can be confirmed that the proposed method has an advantage in signal denoising compared with the other two methods. In particular, the measurement error is only 1%.

### 3.3. Defect detection

#### 3.3.1. Test specimen

In this part, three different rectangular groove defects are tested with a set of different lift-off distance. The diameter of the probe is larger than the width of the defect under test and the ultrasound echo signal contains the bottom echo and defect echo. When lift distance increases, all the echoes were submerged in the noise. The maximum lift-off distance is 1.3 mm. The detailed information of these samples can be found in Table 8.

#### 3.3.2. Result and analysis

Fig. 19, Fig.20 and Fig. 21 shows the visual results of the above algorithms and the thickness of defect to the tested specimen surface.

It can be seen from the results that the proposed algorithm can extract both defects signal and bottom wave signal from the ultrasound echo signal with a strong noise interference when there exists a larger lift-off distance. The proposed methods preserve the characteristics of the echo signal and enhance the weak signal of defects. The processed signal can be used to calculate the thickness of the defect. It can be seen from the results that the error is quite small in different defects detection cases.

### 4. Conclusion and future works

In this paper, an ultrasonic echo model for lift-off effect analysis and a new denoising method based on modified VMD linked wavelet algorithm are proposed. Compared with current state-of-art methods, the proposed method has a better performance in thickness measurement and defects detection for different materials. The proposed method has a higher SNR result. Furthermore, the proposed method has a better performance in extracting thickness information and the envelope is obtained smoother with less noise. The experimental results show that the proposed method can not only eliminate the noise but also preserve the defect information. Future research will focus on the detection of complex defects and automatic identification strategy.



## Acknowledgement

The work was supported by state administration of quality supervision, inspection and quarantine (No. 2017QK042), supported by National Natural Science Foundation of China (No. 61527803), supported by Science and Technology Department of Sichuan, China (Grant No.2018GZ0047 and Grant No.2018JY0655).

## References

- [1] Li Y, Li YF, Wang QL, et al. Measurement and defect detection of the weld bead based on online vision inspection. *IEEE Trans Instrum Meas* 2010;59(7):1841–9.
- [2] Legendre S, Massicotte D, Goyette J, et al. Neural classification of Lamb wave ultrasonic weld testing signals using wavelet coefficients. *Instrumentation & Measurement IEEE Transactions on* 2001;50(3):672–8.
- [3] Liao G, Xi J. Ultrasonic testing signal processing of weld flaw based on the second generation wavelet[C]/ninth international conference on hybrid intelligent systems. *IEEE Computer Society*; 2009. p. 539–42.
- [4] Liu G, Jiang LI, Gan Z, et al. Phased array ultrasonic testing for duplex stainless steel butt weld based on TRL probe. *Nondestructive Testing*; 2018.
- [5] Nakamura N, Ashida K, Takishita T, et al. Inspection of stress corrosion cracking in welded stainless steel pipe using point-focusing electromagnetic-acoustic transducer. *NDT E Int* 2016;83:88–93.
- [6] Kasai N, Takada A, Fukuoka K, et al. Quantitative investigation of a standard test shim for magnetic particle testing. *NDT E Int* 2011;44(5):421–6.
- [7] Fukuoka K, Noma S, Kobayashi M, et al. Consideration of multi-coil type magnetizer for detection of omnidirectional crack in magnetic particle testing. *Int J Appl Electromagn Mech* 2016;52(3):1–8.
- [8] Hou RS, Shao JX, Wang L, et al. Image processing of real-time automatic X-ray inspection system for weld defects. *Nondestructive Testing*; 2009.
- [9] Dong Du, Hou Runshi, Shao Jiaxin, et al. Registration of real-time X-ray image sequences for weld inspection. *Nondestruct Test Eval* 2010;25(2):153–9.
- [10] Hirao M, Ogi H. An SH-wave EMAT technique for gas pipeline inspection. *NDT E Int* 1999;32(3):127–32.
- [11] Ren B, Xin J. In-line inspection of unpiggable buried live gas pipes using circumferential EMAT guided waves[C]/American Institute of Physics Conference Series. American Institute of Physics Conference Series; 2018.
- [12] Dhayalan R, Balasubramaniam K, Krishnamurthy CV, et al. Multi mode lamb waves interaction with defect in metallic structures using EMAT: modeling and experiment [C]/international symposium for research scholars on metallurgy, materials science and engineering. 2018.
- [13] Cunfu HEA. New surface wave EMAT with high SNR and the application for defect detection in thick-walled pipes. *J Mech Eng* 2017;53(4):59.
- [14] Lee JH, Kim DH. Integrity evaluation of pipe welding zones using wavelet transforms, and specific sensitivities based on SH-EMAT pulse-echo method. *Int J Precis Eng Manuf* 2014;15(10):2051–7.
- [15] Yang L, Ume IC. Measurement of weld penetration depths in thin structures using transmission coefficients of laser-generated Lamb waves and neural network. *Ultrasonics* 2017;78:96–109.
- [16] Huang S, Zhao W, Zhang Y, et al. Study on the lift-off effect of EMAT. *Sens Actuators A Phys* 2009;153(2):218–21.
- [17] Le M, Kim J, Kim S, et al. Nondestructive testing of pitting corrosion cracks in rivet of multilayer structures. *Int J Precis Eng Manuf* 2016;17(11):1433–42.
- [18] Kim YY, Kim EH. Effectiveness of the continuous wavelet transform in the analysis of some dispersive elastic waves. *J Acoust Soc Am* 2001;110(110):86–94.
- [19] Legendre S, Goyette J, Massicotte D. Ultrasonic NDE of composite material structures using wavelet coefficients. *NDT E Int* 2001;34(1):31–7.
- [20] Oruklu E, Sanii J. Ultrasonic flaw detection using discrete wavelet transform for NDE applications. *Proc IEEE Ultrason Symp* 2004;2(6):1054–7. 2.
- [21] Liang W, Que PW. Optimal scale wavelet transform for the identification of weak ultrasonic signals. *Measurement* 2009;42(1):164–9.
- [22] Wu M, Zhang H, Sun Z, et al. Application of wavelet analysis and artificial neural network pattern recognition to flaw classification in ultrasonic testing. *J China Inst Min Technol* 2000;27(3):149–59.
- [23] Cruz FC, Simas Filho EF, Albuquerque MC, et al. Efficient feature selection for neural network based detection of flaws in steel welded joints using ultrasound testing. *Ultrasonics* 2017;73:1–8.
- [24] Huang NE, Shen Z, Long SR, et al. The empirical mode decomposition and the Hilbert spectrum for nonlinear and non-stationary time series analysis. *Proc R Soc Lond Ser A Math Phys Eng Sci* 1998;454(1971):903–95.
- [25] Sun M, Shen Y, Zhang W. A wavelet threshold denoising method for ultrasonic signal based on EMD and correlation coefficient analysis[C]/International Congress on Image and Signal Processing. *IEEE*; 2010. p. 3992–6.
- [26] Kubik T, Kałczyński K, Cygan S, et al. Evaluation of the empirical mode decomposition method as a tool for preprocessing ultrasonic cardiological data. 2014.
- [27] Zhaohua WU, Norden E, Huang. Ensemble empirical mode decomposition: a noise-assisted data analysis method. *Adv Adapt Data Anal* 2009;1(01).
- [28] Nie Z, Wang K, Zhao M. Application of wavelet and EEMD joint denoising in nonlinear ultrasonic testing of concrete. 2018.
- [29] Yu JM, Zhang Z. Research on feature extraction for ultrasonic echo signal based on EEMD approach. *Appl Mech Mater* 2013;321–324:1311–6.
- [30] Dragomiretskiy K, Zosso D. Variational mode decomposition. *IEEE Trans Signal Process* 2014;62(3):531–44.
- [31] Liu C, Zhu L, Ni C. Chatter detection in milling process based on VMD and energy entropy. *Mech Syst Signal Process* 2018;105:169–82.
- [32] Zhang X, Miao Q, Zhang H, et al. A parameter-adaptive VMD method based on grasshopper optimization algorithm to analyze vibration signals from rotating machinery. *Mech Syst Signal Process* 2018;108:58–72.
- [33] Lee JH, Kim DH. Integrity evaluation of pipe welding zones using wavelet transforms, and specific sensitivities based on SH-EMAT pulse-echo method. *Int J Precis Eng Manuf* 2014;15(10):2051–7.
- [34] ang K, Peng C, Zhang Y, et al. A de-noising algorithm for EMAT on wheels[M]/nondestructive testing of materials and structures. 2013.
- [35] Ribichini R, Nagy PB, Ogi H. The impact of magnetostriction on the transduction of normal bias field EMATs. *NDT E Int* 2012;51(10):8–15.